# Size normalizing planktonic Foraminifera abundance in the water column

Sonia Chaabane, Thibault de Garidel-Thoron, Xavier Giraud, Julie Meilland, Geert-jan Brummer, Lukas Jonkers, P. Graham Mortyn, Mattia Greco, Nicolas Casajus, Michal Kucera, et al.

LIMNOLOGY and OCEANOGRAPHY: METHODS

ASLO

*Limnol. Oceanogr.: Methods* 2024

doi: 10.1002/lom3.10637

# Size normalizing planktonic Foraminifera abundance in the water column

**Sonia Chaabane**,[1,2,3]* **Thibault de Garidel-Thoron**,[1] **Xavier Giraud**,[1] **Julie Meilland**,[4] **Geert-Jan A. Brummer**,[5] **Lukas Jonkers**,[4] **P. Graham Mortyn**,[6] **Mattia Greco**,[7] **Nicolas Casajus**,[3] **Michal Kucera**,[4] **Olivier Sulpis**,[1] **Azumi Kuroyanagi**,[8] **Hélène Howa**,[9] **Gregory Beaugrand**,[10] **Ralf Schiebel**[2]

[1]Aix-Marseille Université, CNRS, IRD, INRAE, CEREGE, Aix-en-Provence, France
[2]Department of Climate Geochemistry, Max Planck Institute for Chemistry, Mainz, Germany
[3]Fondation Pour la Recherche sur la Biodiversité (FRB-CESAB), Montpellier, France
[4]MARUM, Center for Marine Environmental Sciences, University of Bremen, Bremen, Germany
[5]Department of Ocean Systems, NIOZ, Royal Netherlands Institute for Sea Research, Texel, The Netherlands
[6]Department of Geography, ICTA, Universitat Autònoma de Barcelona, Barcelona, Spain
[7]Institute of Marine Sciences (ICM), CSIC, Passeig Marítim de la Barceloneta, Barcelona, Spain
[8]Tohoku University Museum, Tohoku University, Sendai, Japan
[9]LPG-BIAF, UMR-CNRS 6112, University of Angers, Angers, France
[10]Université Littoral Côte d'Opale, Univ. Lille, CNRS, UMR 8187, LOG, Laboratoire d'Océanologie et de Géosciences, Lille, France

## *Abstract*

Planktonic Foraminifera have been collected from the water column with different plankton sampling devices equipped with nets of various mesh sizes, which impedes direct comparison of observed quantifications. Here, we use data on the community size structure of planktonic Foraminifera to assess the impact of mesh size on the measured abundance (ind $m^{-3}$) of planktonic Foraminifera. We use data from the FORCIS database (Chaabane et al., 2023, Scientific Data **10**: 354) on the global ocean at different sampling depths over the past century. We find a global cumulative increase in abundance with size, which is best described using a Michaelis–Menten function. This function yields multiplication factors by which one size fraction can be normalized to any other size fraction equal to or larger than 100 $\mu$m. The resulting size normalization model is calibrated over a range of different depth intervals, and validated with an independent dataset from various depth ranges. The comparison to Berger's (1969, Deep. Res. Oceanogr. Abstr. **16**: 1–24) equivalent catch approach shows a significant increase in the predictive skill of the model. The new size normalization scheme enables comparison of Foraminifera abundance data sampled with plankton nets of different mesh sizes, such as compiled in the FORCIS database. The correction methodology may be effectively employed for various other plankton groups such as diatoms and dinoflagellates.

*Correspondence: sonia.chaabane@gmail.com; chaabane@cerege.fr; sonia.chaabane@mpic.de

**Author Contribution Statement:** The study was designed by SC, XG, TG-T, RS, JM, GB, LJ, and GM. The data analysis was carried out by SC and XG generated the equations. All authors contributed to the interpretation and discussion of the results. SC wrote the paper with contributions from TG-T, RS, JM, GB, LJ, GM, MG, and OS.

Additional Supporting Information may be found in the online version of this article.



Planktonic Foraminifera are ubiquitous marine unicellular mesoplankton calcifiers, contributing to the global carbon cycle by exporting carbon to the seafloor. They live in the upper hundreds of meters of the ocean (Rebotim et al. 2017) where they grow by sequential addition of calcareous chambers to their shell (called tests), ranging from ~ 100 $\mu$m to ~ 1 mm, varying across species. While calcifying, Foraminifera encode ambient environmental conditions in their shells, enabling key proxies for paleoceanographic reconstructions. Upon death or reproduction, the empty shells sink through the water column to the ocean floor where they accumulate and eventually fossilize (Bé and Anderson 1976; Hemleben et al. 1989). Their ocean-wide distribution, species diversity, and shell geochemistry (isotope and trace metal composition)

facilitate the reconstruction of past ocean and climate conditions using sedimentary records (e.g., Anderson and Prell 1993; Bé 1977; Bonneau et al. 1980; Caulet et al. 1992; CLIMAP 1976; Ganssen and Kroon 1991; de Garidel-Thoron et al. 2005; Grazzini et al. 1995; Kroon and Ganssen 1989; Kucera et al. 2005; Mortyn and Martinez-Boti 2007; Steens et al. 1992; Strack et al. 2022).

Planktonic Foraminifera begin their life with a single initial calcified chamber, the proloculus, which ranges 5–50 $\mu$m in diameter (Sverdlove and Bé 1985; Brummer et al. 1987). The calcified shell which houses the cytoplasm grows by adding chambers to the test. The final size of the adult shell varies between species and is affected by the ecological conditions any individual experiences during its ontogeny (Hecht 1976; Schmidt et al. 2004). Therefore, the size spectrum of the planktonic Foraminifera community at a specific location and time is indicative of the present species, their average maturity levels and fitness with the environmental parameters. When collecting samples with a mesh larger than the smallest specimens, both the number of individuals per volume of seawater and species composition data will be skewed, as smaller specimens will be missed (Berger 1969; Berger 1971; Bé and Hutson 1977; Brummer and Kroon 1988).

Over the last century, living planktonic Foraminifera were collected from the water column using various devices equipped with nets of different mesh sizes (30–650 $\mu$m). Originally, samples were collected with coarse-meshed nets and gradually changed over time to finer nets that caught smaller specimens and species. For instance, King and Demond (1953) used a mesh size of 650 $\mu$m whereas Bé et al. (1985) and Bé and Hemleben (1970) used mesh sizes of 333 and 202 $\mu$m, respectively. More recent studies have used smaller mesh sizes from 30 $\mu$m up to the classical 150 $\mu$m sieve size traditionally used in paleoceanographic studies (e.g., Boltovskoy et al. (2000), 30 μm; Keigwin et al. (2005), 63 μm; Kuroyanagi and Kawahata (2004), Lessa et al. (2020), Mallo et al. (2017), 125 μm; Schiebel et al. (1995), 100 μm; Sousa et al. (2014), Ufkes et al. (1998), 150 μm). The lack of standardized methodologies in plankton net studies complicates the comparison of data across different sampling efforts.

The resulting sampling bias in measuring planktonic Foraminifera abundances not only distorts our understanding of their contribution to the oceanic carbon cycle but also hampers efforts to define their ecological niches. Despite numerous studies recognizing the impact of mesh size on the observed species abundance and diversity, few have specifically addressed this bias (Berger 1969; Peeters et al. 1999; Schiebel and Hemleben 2000). In a pioneering study, Berger (1969) derived a set of equations to compute equivalent catches for different mesh sizes. The equations were based on a limited range of samples and used assumptions such as the invariance of the assemblage composition through space and time, or that the size mode of the catch corresponds to the mesh size used. Since the 1960s, a wealth of new data have become available and recently synthesized in the FORCIS database (Foraminifera Response to Climatic Stress database, de Garidel-Thoron et al. 2022; Chaabane et al. 2023), allowing us to explore the possibility to design a better-constrained normalization approach. The availability of large datasets is fundamental to fully compare samples collected using different mesh sizes (Supporting Information Fig. S2), which need to be normalized at a similar mesh size (e.g., larger than 100 $\mu$m).

In the FORCIS database, abundance data are compiled as size-fractionated abundance data, called subsample, and are available for thousands of individual samples. For instance, from a single sample split into six size fractions (100–125, > 125–150, > 150–200, > 200–250, > 250–315, and > 315 $\mu$m), the finer size fraction (encompassing the three size classes 100–125, > 125–150, and > 150–200 $\mu$m) presents the highest abundance (Supporting Information Fig. S1).

The objective of this study is to propose a model to normalize the abundance (ind $m^{-3}$) of planktonic Foraminifera caught in a net of a given mesh size to the abundance that would be measured if a net with another mesh size was used instead, allowing us to relate all counts to a standard mesh size. We assess the sensitivity of this model, normalized to sizes equal to or larger than 100 $\mu$m, to different water depths, seasons, oceanic basins, and species size categories within the training set. The predictive skill of our model is validated using a large, independent, size-fractionated validation dataset from the North Atlantic Ocean (Retailleau et al. 2011). Lastly, we compare the predictions of this model with the only analogous normalization methodology developed by Berger (1969) on planktonic Foraminifera. Our normalization approach is applied to global observations on samples from plankton nets, plankton pumps, and Continuous Plankton Recorders (CPRs) to derive a size harmonized estimate of planktonic Foraminifera abundance. The correction methodology is applicable not only to planktonic Foraminifera but could be adapted to correct for mesh size bias in other plankton groups sampled using similar methods, such as pteropods or other taxa.

## Materials and procedures

### Size-normalized catch

#### *Model training dataset*

For this analysis, we select a subset of samples collected by plankton nets from the FORCIS database (Chaabane et al. 2023) and fractionated into different size fractions, to characterize the relationship between abundances and the size fractions of Foraminifera tests. A total of 1026 samples match this criterion and were sieved and separated into 6 different size fractions ($k$ from 1 to 6), where $k_{max}$ is the number of the last size class within a single subsample (an aliquot plankton sample obtained from a specific depth range, time interval, size fraction range, and location) for each of the following mesh size fractions: > 100–125 $\mu$m ($k = 1$), > 125–150 $\mu$m ($k = 2$), > 150–200 $\mu$m ($k = 3$), > 200–250 $\mu$m

($k = 4$), > 250–315 $\mu$m ($k = 5$), > 315 $\mu$m ($k = 6$). Due to varying methodologies for identifying living foraminifera over the last decades, such as Rose Bengal staining and visual cytoplasm detection, and the associated uncertainties (Corliss and Emerson 1990; Bernhard 2000), we chose to analyze both living and dead specimens together to ensure consistency in our findings. Thus, the selected samples contain both cytoplasm-filled and empty planktonic Foraminifera tests sampled from the North Atlantic, Indian and Arctic Oceans (Fig. 1), and cover a depth range of 0–1000 m water depth.

### *Multiplication factor calculation*

The cumulative abundance ($C_{\text{cum}}$; in individuals $\text{m}^{-3}$) refers to the total abundance (defined as the number of individuals per cubic meter) across a range of size fractions. For size classes ranging from size class 1 (100–125 $\mu$m) to class $k$, the cumulative abundance, $C_{\text{cum},k}$, is calculated as follows:

$$C_{\text{cum},k} = \sum_{i=1}^{k} C_i$$

where $C_i$ is the abundance in size fraction $i$.

Observations indicate that the cumulative abundance typically exhibits an asymptotic shape (Fig. 2a). This behavior is quantified through a multiplication factor $f_k$, defined as the ratio of the cumulative abundance for a given class $k$ to the abundance of the first class ($C_1$):

$$f_k = \frac{C_{\text{cum},k}}{C_1} \quad (1)$$

The selection of a fitting function for the multiplication factor must adhere to the principle of parsimony, implying a limited number of parameters for calibration to avoid overfitting. Additionally, the function should asymptote to a maximum value, reflecting the biological reality that a population's total abundance cannot be infinite and that there are no more individuals above a certain size. The chosen function's parameters should also correlate with the distribution patterns of size vs. abundance within specific Foraminifera populations.

To accurately model the gradual increase and eventual plateau of the cumulative distribution starting from a nonzero initial class size, we sought a fitting function that depicts this pattern without overemphasizing smaller size fractions. Among the considered alternatives, the logistic function, while commonly used, seems inadequate due to its inability to constrain the lower range effectively, particularly evident in our study where not all size spectra were covered by our mesh sizes.

Therefore, the Michaelis–Menten (MM) function (Michaelis and Menten 1913; English version, Johnson and Goody 2011), traditionally linked to enzyme kinetics but broadly applicable to various biological phenomena demonstrating an asymptotic behavior, was selected as the most suitable fitting function. This decision was supported by its demonstrated effectiveness

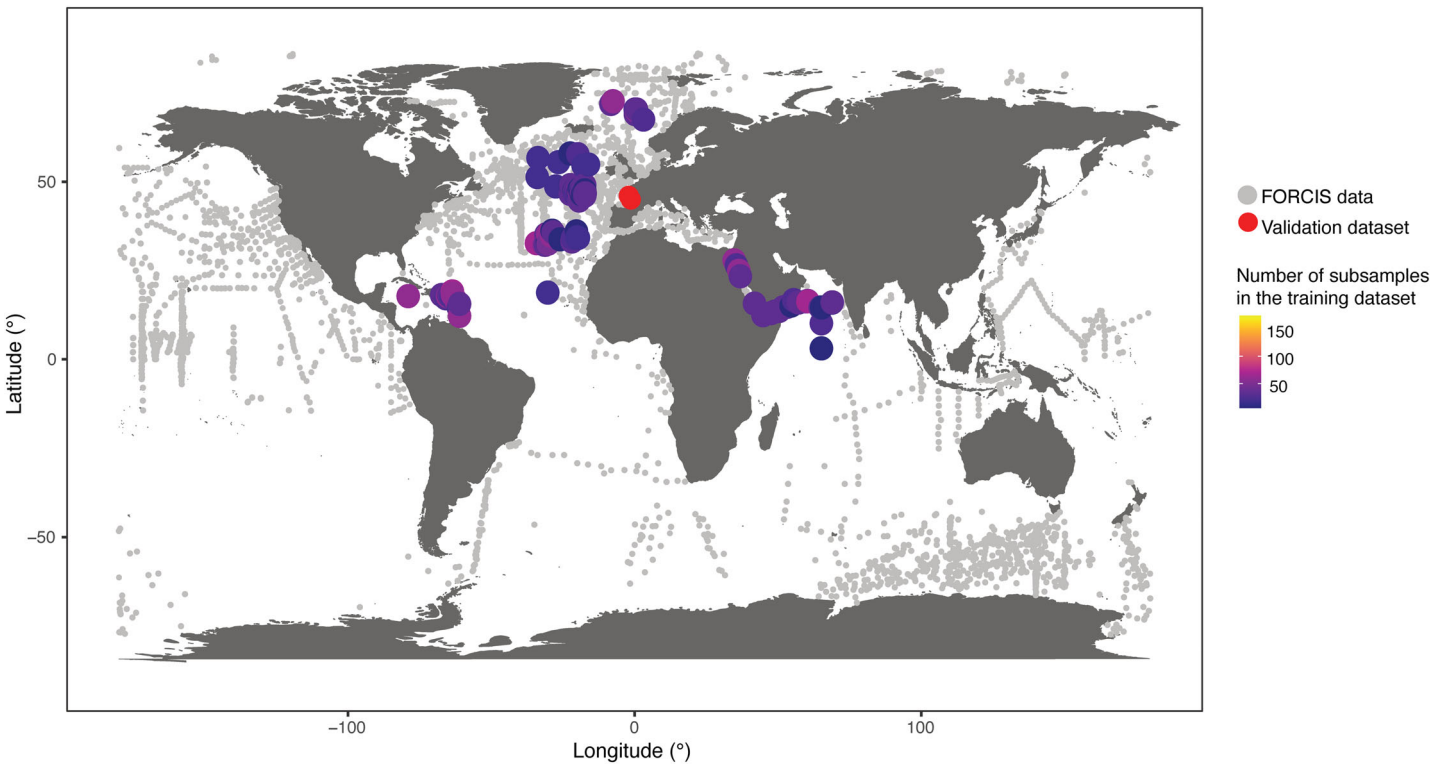


**Fig. 1.** Sampling location of the FORCIS data, training dataset and Retailleau et al. (2011) data.

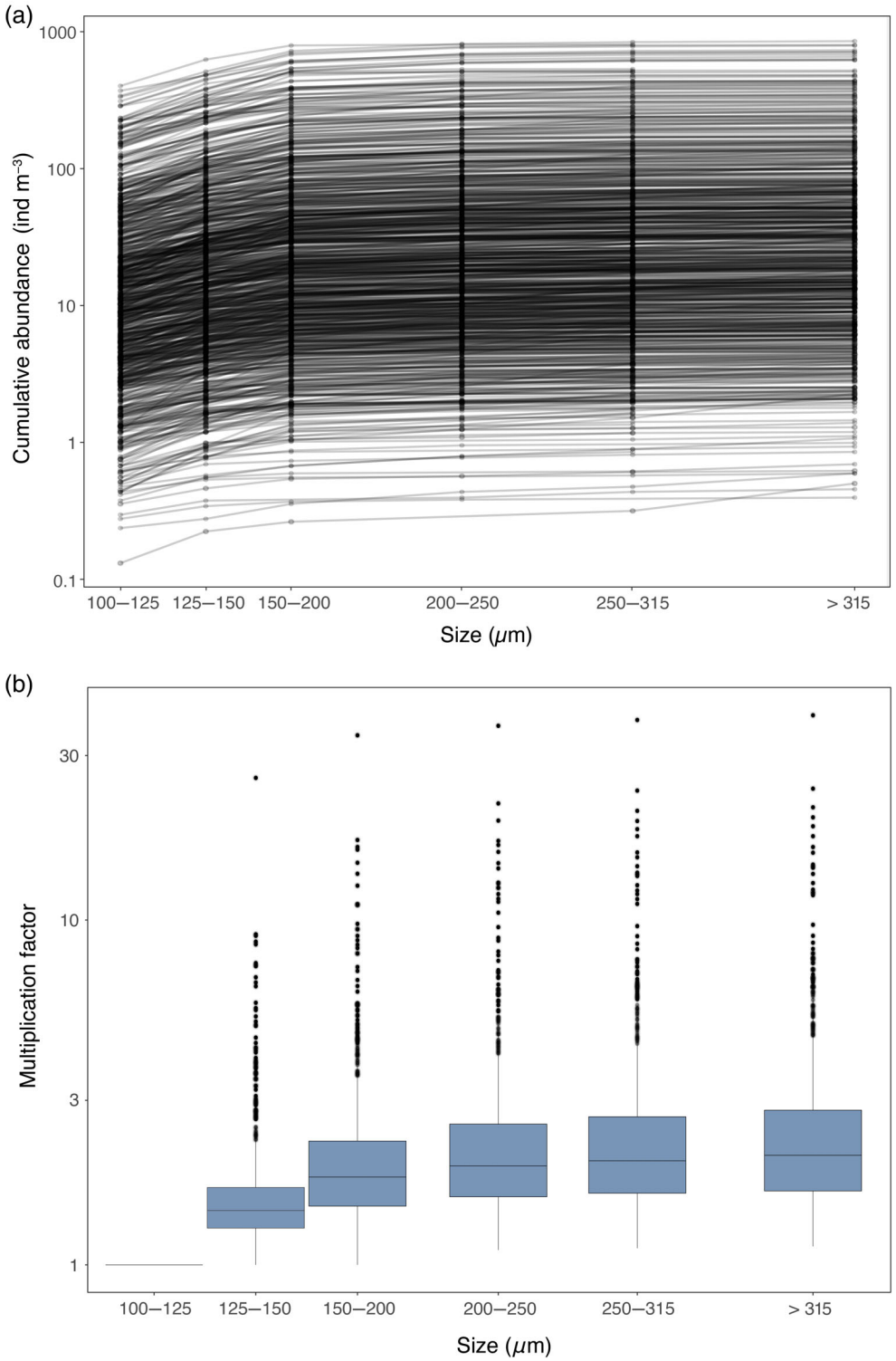


**Fig. 2.** (**a**) The cumulative abundance frequency vs. the size fractions (100–125, > 125–150, > 150–200, > 200–250, > 250–315, > 315–400, > 400–500 and > 500 $\mu$m). Each black line represents a sample. (**b**) Box plot representing the multiplication factor curves calculated using Eq. 1 vs. each size fraction (> 100–125, > 125–150, > 150–200, > 200–250, > 250–315, >315–400, >400–500 and > 500 $\mu$m). Black dots are the outliers.

in other biological contexts, such as growth modeling studies (Hohenegger et al. 2014; Sardari 2023; Walters et al. 2024). The MM function's adaptability stems from its simplicity, encapsulating the dynamics of planktonic Foraminifera test size distributions with only two parameters: the maximum potential abundance ($f_{\max}$) and the initial response rate or

sharpness of the curve ($S_{half}$) at the beginning of the distribution.

The MM function facilitates a nuanced interpretation of Foraminifera population distributions, particularly in the context of size ranges. The $f_{max}$ parameter, indicating the maximum multiplication factor achievable between the smallest size class (100–125 $\mu$m) and the total population abundance, reflects the breadth of the size distribution. Higher $f_{max}$ values suggest a significant contribution from larger specimens to the population's total abundance. Conversely, the half-saturation constant ($S_{half}$), quantifies the distribution curve's steepness. Lower $S_{half}$ values indicate a rapid attainment of the maximum abundance, emphasizing the dominance of smaller size fractions within the population.

By applying a scale translation to the initial size range, we derive a model for the multiplication factor as follows (Fig. 3):

$$f_k = 1 + (f_{max} - 1)\frac{(S_{sup,k} - S_{sup,1})}{(S_{sup,k} - S_{sup,1}) + (S_{half} - S_{sup,1})} \quad (2)$$

where $S_{sup,1}$ and $S_{sup,k}$ are the upper size limits of size class 1 and $k$, respectively, and $S_{half}$ and $f_{max}$ are the fitted parameters.

To derive $S_{half}$ and $f_{max}$, we fit $f_k$ to $S_{sup,k}$ through a MM equation, using the "MM.2()" function of the drc package in R (Ritz et al. 2015).

### *Size-normalized catch model*

Finally, to scale the measured abundance from any given size range ($C^{sz\_sup}_{sz\_inf}$, with sz_inf and sz_sup being the lower and upper limits of the size fraction, given in micrometers, $\mu$m) to the theoretical abundance at a size range extending from a chosen normalizing value ($C^{\infty}_{sz\_norm}$), the following equation is applied:

$$C^{\infty}_{sz\_norm} = C^{sz\_sup}_{sz\_inf}\frac{f_{max} - f_{sz\_norm}}{f_{sz\_sup} - f_{sz\_inf}} \quad (3)$$

where sz_inf and and sz_sup are the lower and upper size limits, respectively, of the measured size fraction, sz_norm is the normalization size and $f_{Sz}$ is the multiplication factor associated to the Sz, computed as follows:

$$\text{if } Sz = 100\,\mu m, \qquad f_{100} = 0$$

$$\text{if } Sz \in [125; +\infty], \quad f_{Sz} = 1 + (f_{max} - 1)\frac{(Sz - S_{125})}{(Sz - S_{125}) + (S_{half} - S_{125})} \quad (4)$$

$$\text{with } S_{125} = 125\,\mu m$$

$$\text{if } Sz \equiv \infty, \quad f_{\infty} = f_{max}$$

The size fractions of 100 and 125 $\mu$m used in this formula are dictated by the finer size class selected for calibration in the database collection, so that the size-normalization (Eq. 3) can be applied to 100 $\mu$m or any size above 125 $\mu$m.

As shown in Fig. 3c, for the distribution of the abundance between 100 and 125 $\mu$m, normalization is possible by extending the calculation of the multiplication factor as follows:

$$\text{if } Sz \in [100; 125], \quad f_{Sz} = \frac{Sz - S_{100}}{S_{125} - S_{100}} \quad (5)$$

Before determining the parameters $S_{half}$ and $f_{max}$, we removed outliers (10% of the data below and above the high-density curves), detected on the multiplication factor of each size fraction, considering values beyond 1.5 times the interquartile range from the median as outliers. The Median + 1.5 * IQR (interquartile range) method, commonly used in box plots to spot outliers, sets a boundary indicating where most data points should lie within a box plot. This boundary is calculated by adding 1.5 times the interquartile range (IQR) to the median. If data points exceed this boundary, they are flagged as potential outliers. Typically, outliers are defined or any value exceeding 1.5 * IQR + Q3 (Freedman et al. 2007). This method is preferred for its ability to handle extreme values and skewed distributions effectively, offering a balanced way to identify outliers while safeguarding the integrity of the data. We used the function "boxplot.stat()" in R (version 2021.09.1; R Core Team 2021) for the detection. The very low abundances in all size classes (flat fit), unrealistically high values in fine size fractions (likely due to technical failure or sampling effects such as clogging of the plankton net) followed by very low abundances in the coarser size fraction, were detected as outliers (Fig. 2b).

Both parameters ($S_{half}$ and $f_{max}$) were determined for each ocean basin where we have the selected data to conceptualize the model (Arctic, North Atlantic, and Indian Oceans), season and water depth interval (between 0–50 m, 50–100 m, 100–300 m, and 300–1000 m), based on the mean depth of the sample to check whether the MM parameters are time and/or space dependent (Supporting Information Table S2; Fig. S3). It was also assessed for three size classes based on adult test size, categorized as small (100200 $\mu$m), medium (>200 to 300 $\mu$m), and large (>300 $\mu$m) species (Table 1; Schiebel and Hemleben 2017).

### *Validation*

To assess the robustness of the proposed model, the obtained Eq. 5 was applied to an independent validation dataset (included in the FORCIS database), that is not part of the training dataset (Fig. 1). This validation set includes 552 subsamples analyzed in three different size fractions, that is, 100–150, > 150–315, and > 315 $\mu$m, where abundances in the > 100 $\mu$m net samples were counted from 0 to 700 m (Retailleau 2009; Retailleau et al. 2011).

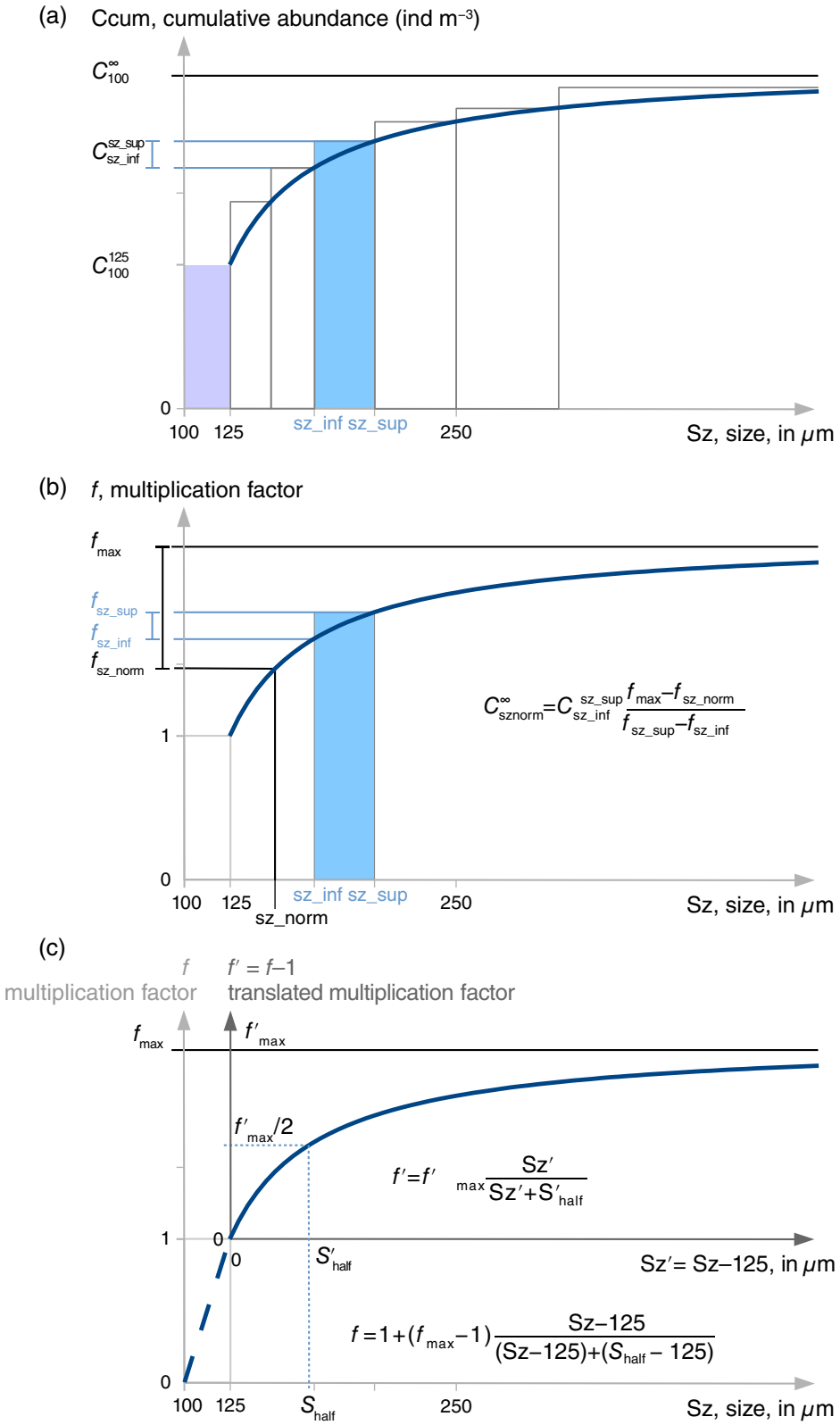


**Fig. 3.** Schematic illustration of the size-normalized catch model. (**a**) Cumulative abundances vs. size fractions. (**b**) Multiplication factors vs. size fractions. (**c**) Multiplication factors and translations to determine the parameters of the Michaelis–Menten fit.

**Table 1.** Planktonic Foraminifera species included in the FORCIS dataset and categorized by their typical adult size: < 200 $\mu$m classified as small, 200–300 $\mu$m as medium, and > 300 $\mu$m as large (Schiebel and Hemleben 2017; Meilland et al. 2021; Brummer and Kučera 2022; Meilland et al. 2022).

| Species name | Average adult size ($\mu$m) | Adult size category |
|---|---|---|
| *Berggrenia pumilio* | 110 | Small |
| *Dentigloborotalia anfracta* | 150 | Small |
| *Globorotalia cavernula* | 170 | Small |
| *Globigerinita minuta* | 110 | Small |
| *Globoturborotalita rubescens* | 150 | Small |
| *Globigerinoides tenellus* | 160 | Small |
| *Globigerinita uvula* | 160 | Small |
| *Neogallitellia vivans* | 150 | Small |
| *Orcadia riedeli* | 110 | Small |
| *Turborotalita clarkei* | 110 | Small |
| *Tenuitellita fleisheri* | 130 | Small |
| *Turborotalita humilis* | 140 | Small |
| *Tenuitellita iota* | 140 | Small |
| *Tenuitellita parkerae* | 140 | Small |
| *Turborotalita quinqueloba* | 180 | Small |
| *Candeina nitida* | 300 | Medium |
| *Globigerina bulloides* | 300 | Medium |
| *Globigerinoides conglobatus* | 300 | Medium |
| *Globigerinoides elongatus* | 250 | Medium |
| *Globigerina falconensis* | 280 | Medium |
| *Globigerinita glutinata* | 220 | Medium |
| *Globorotaloides hexagona* | 250 | Medium |
| *Globorotalia hirsuta* | 300 | Medium |
| *Globorotalia inflata* | 300 | Medium |
| *Globigerinoides ruber any* | 250 | Medium |
| *Globigerinoides ruber ruber* | 250 | Medium |
| *Globorotalia scitula* | 230 | Medium |
| *Globorotalia theyeri* | 280 | Medium |
| *Pulleniatina obliquiloculata* | 300 | Medium |
| *Trilobatus sacculifer* | 300 | Medium |
| *Neogloboquadrina incompta* | 200 | Medium |
| *Neogloboquadrina pachyderma* | 200 | Medium |
| *Globoquadrina conglomerata* | 300 | Medium |
| *Globorotalia crassaformis* | 300 | Medium |
| *Neogloboquadrina dutertrei* | 300 | Medium |
| *Globorotalia tumida* | 280 | Medium |
| *Globorotalia ungulata* | 300 | Medium |
| *Globorotalia cultrata* | 320 | Large |
| *Globorotalia truncatulinoides* | 400 | Large |
| *Beella digitata* | 400 | Large |
| *Globigerinella adamsi* | 350 | Large |
| *Globigerinella siphonifera* | 320 | Large |
| *Hastigerinella digitata* | 800 | Large |
| *Hastigerina pelagica* | 800 | Large |
| *Orbulina universa* | 600 | Large |
| *Globigerinella calida* | 320 | Large |
| *Sphaeroidinella dehiscens* | 320 | Large |

### Berger's "equivalent catch"

Since the use of different mesh sizes could yield different faunal compositions for the same sample, Berger 1969 defined the "equivalent catch" to compare the abundances of planktonic Foraminifera collected with plankton nets of unequal mesh size. The standardized abundance of planktonic Foraminifera would then be obtained using the following empirical equation (Eq. 6):

$$\text{Abundance}_{(\text{standardized})} = \text{Abundance}_{(\text{actual})} \times \left( \frac{S_{(\text{actual})}}{S_{(\text{standardized})}} \right)^{a} \quad (6)$$

where $S_{(\text{actual})}$ is the observed (net or sieve) mesh size used, $S_{(\text{standardized})}$ is the standard mesh size, and $a$ is a constant number set to 3 for plankton tow samples (Berger (1969) and Peeters et al. (1999)).

To compare the equivalent catch using the Berger (1969) equation to the size-normalized catch defined in this study, we used the size-fractionated training dataset (5117 subsamples extracted from the FORCIS database) separated into six different size fractions (> 100–125, > 125–150, > 150–200, > 200–250, > 250–315, and > 315 $\mu$m). Then, we calculated the abundance at different equivalent mesh sizes (> 100, > 125, > 150, > 200, > 250, and > 315 $\mu$m), as computed by the equivalent catch formula in Berger (1969). The obtained abundances were then standardized to 100 $\mu$m and therefore used "100" as $S_{(\text{standardized})}$ in Eq. 6 and to a known abundance (> 100 $\mu$m).

The coefficient of determination ($r^2$) of the linear regression models were calculated through the R scripts using the "ggpmisc" packages, to investigate the similarity between the values calculated using the Berger (1969) equation (Eq. 6) and our approach (Eq. 4).

### Application of the size-normalized catch model

We extracted more than 175,000 subsamples of species counts from the FORCIS database (Chaabane et al. 2023), that is, single species aliquots collected within a depth range, time interval, and size fraction range at a given location. Subsamples include counts on the total of cytoplasm-filled and empty tests in a defined water parcel. The subsamples include data published between 1950 and 2018 and collected in different oceanographic environments by continuous plankton

recorders (CPR; 157,000 samples having 157,000 subsamples), plankton nets (6000 samples having 19,000 subsamples), and plankton pump (300 samples having 400 subsamples) in the Atlantic, Pacific, Indian, and Arctic Oceans (Supporting Information Fig. S2). The various types of counts (raw data or relative abundance) for total planktonic Foraminifera and species-specific count data within these samples were extracted from the FORCIS database (Supporting Information Fig. S3). Only samples containing information regarding both the total number of individuals and the filtered volume were considered for conversion to abundances (ind $m^{-3}$). All CPR data have only one subsample per sample and were collected only between 5 and 10 m water depth using a mesh size of 270 $\mu$m.

The corresponding season at the time of the collection of each sample was extracted from the FORCIS database. Seasons were distinguished between the Northern and Southern Hemispheres. In the Northern Hemisphere, autumn comprises September, October, and November; winter includes December, January, and February; spring consists of March, April, and May; and summer spans June, July, and August. Conversely, in the Southern Hemisphere, the seasons are reversed: spring occurs in September, October, and November; summer in December, January, and February; autumn in March, April, and May; and winter in June, July, and August.

## Results

### FORCIS size-normalized catch

#### *Sieve size and abundance*

The relationships between abundances of planktonic Foraminifera, water depth, and size fraction have been assessed using the cumulative abundances as a function of size fraction in each sample (Fig. 2a). Despite the large differences between samples, they show similar and parallel patterns over a wide range of abundances (Fig. 2a), with a notable feature: the cumulative abundance is higher for the samples from shallow waters compared to their deep-water counterparts (Fig. 4a). The pattern of the cumulative curves closely resembles that of a logarithmic function, exhibiting the most pronounced increases in the finer fractions (100–125 and 125–150 $\mu$m), which then level off as the size fractions become coarser. The cumulative abundances range between 0.2 and 600 ind $m^{-3}$ for the finer size fractions (100–125 and 125–150 $\mu$m) and between 4 and 900 ind $m^{-3}$ for the coarser ones.

The multiplication factors (by which the abundances increase in each size fraction) derived from the cumulative abundance curves (*see* Materials and procedures), show an overall asymptotic pattern across all samples (Fig. 2b). The latter is similar to the Michaelis–Menten curve with constants $S_{\text{half}}$ and $f_{\text{max}}$ obtained for the general fit of about $178 \pm 3$ $\mu$m and $2.48 \pm 0.02$, respectively (Fig. 4b; Table 2).

A steep slope in multiplication factor is observed between 100 and 150–200 $\mu$m for all curves, and levels off for size fractions larger than 250 $\mu$m. Generally, the mean value of the factor ($f_k$) is about 1.47 for the >125–150 $\mu$m size fraction and reaches 1.85 for the size fraction >150–200 $\mu$m, increasing to 2.21 for the size fraction larger than 315 $\mu$m. The increase of $f_k$ between the size fractions >200–250 and >250–315 $\mu$m is low and close to 0.11.

The obtained asymptotic curves (multiplication factors vs. size fractions) also show similar patterns for each water depth (0–50, >50–100, >100–300, >300–1000, and >1000 m) with a steep slope between 100 and 150 $\mu$m (Fig. 4b). The constants of these MM fits range between 167–186 and 2.18–2.75 $\mu$m for $S_{\text{half}}$ and $f_{\text{max}}$, respectively. Highest values are observed at the shallower depths (from 2.54 to 2.75 and from 184 to 186 $\mu$m for $f_{\text{max}}$ and $S_{\text{half}}$, respectively), between 0 and 100 m, especially in the coarser size fractions (Table 2).

Between 100 and 150 $\mu$m, the multiplication factor is the same at all depths (Table 3), while the difference between two successive multiplication factors at all depths is decreasing at coarser sizes. For instance, the difference between two successive multiplication factors is low for the size fractions >250 $\mu$m, and particularly low for the size fractions >315 $\mu$m, where the abundance is also close to 0.

In deeper samples, the coarse fraction shows lower abundances than in shallow waters (Fig. 4). For example, for the size fraction >315 $\mu$m the standard deviation among the multiplication factors is 0.16, while it is only 0.03 for the size fraction >125–150 $\mu$m (Table 3).

The relationships between the multiplication factors derived from the cumulative abundance curves and the size fractions were assessed per season, ocean basin, and water depth interval (Fig. 5). Overall, the resulting envelopes (confidence intervals at the limits of 2.5% and 97.5%) show similar parallel patterns with higher uncertainty at larger sizes, especially for the North Atlantic Ocean data in summer, spring, and autumn, where the number of data points is high. However, these envelopes overlap for the Indian and Arctic Oceans in all seasons, where the sampling coverage is low (e.g., Indian Ocean summer observations are 80% lower than in the North Atlantic Ocean). Overall, if MM parameters vary slightly between ocean basins and seasons (Fig. 5b–d; Supporting Information Table S2), the differences cannot be thoroughly confirmed in this study due to the sampling coverage. The depth dependance of the MM parameters is the factor that is shown to be robust in our analyses. Consequently, our analyses rely on globally derived MM parameters across depth intervals.

#### *Species test size and abundance*

Test sizes of adult specimens (Table 1) differ significantly among species and thus impact the distribution of abundances with sieve size. Typically, small-sized species, such as *Berggrenia pumilio*, *Dentigloborotalia anfracta*, *Globigerinita glutinata*, *Globigerinita minuta*, *Globoturborotalita rubescens*,

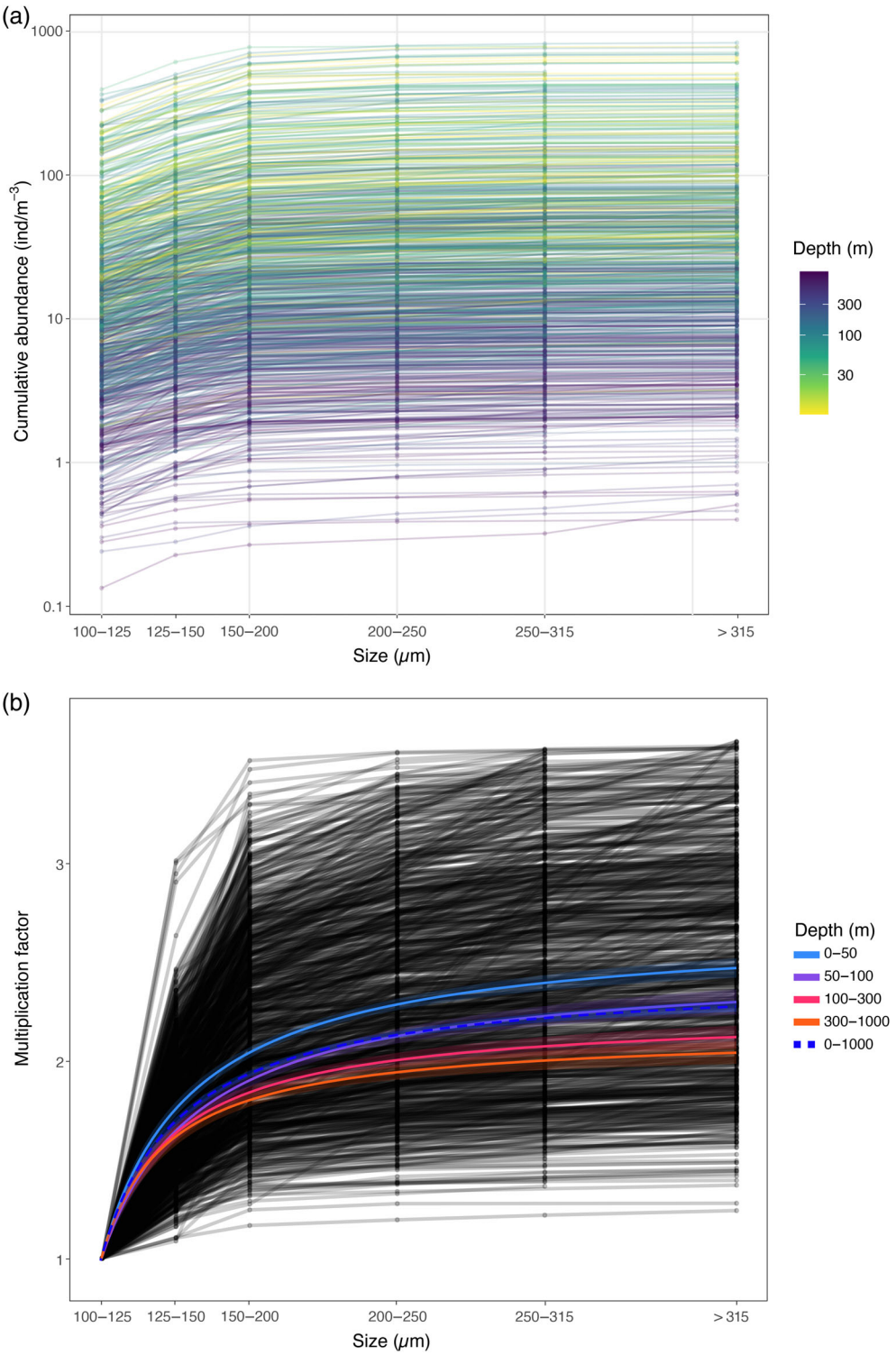


**Fig. 4.** (**a**) Cumulative abundance per plankton tow sample of the training dataset calculated at each size fraction (100–125, > 125–150, > 150–200, > 200–250, > 250–315, > 315–400, > 400–500, and > 500 $\mu$m) per each sample (black lines). Line colors indicate depth intervals. (**b**) Multiplication factor curves calculated using Eq. 1 vs. size fraction in each sample (black lines). The general Michaelis–Menten fit was obtained on the global data (dashed blue line), and for each depth range.

**Table 2.** Estimation parameters $f_{max}$ and $S_{half}$ generated for each depth interval using the training dataset.

| Depth interval (m) | $S_{half}$ ($\mu$m) | $f_{max}$ |
|---|---|---|
| 0–1000 | 178 ± 3 | 2.48 ± 0.02 |
| 0–50 | 184 ± 5 | 2.75 ± 0.05 |
| 50–100 | 186 ± 7 | 2.54 ± 0.06 |
| 100–300 | 171 ± 6 | 2.30 ± 0.05 |
| 300–1000 | 167 ± 6 | 2.18 ± 0.05 |

*Globoturborotalita tenellus*, *Globigerinita uvula*, and *Gallitellia vivans*, may not be found at all in medium to coarse mesh sizes. In contrast, large-sized species occur in all size fractions, such as *Globigerinella adamsi*, *Globorotalia cultrata*, *Beella digitata*, *Globorotalia truncatulinoides*, *Hastigerinella digitata*, and *Hastigerina pelagica*. Medium-sized species like *Candeina nitida*, *Globigerina bulloides*, and *Globorotalia scitula* occur in small (100–200 $\mu$m), medium (> 200–300 $\mu$m), but are often not found in the very large size fractions (> 300 $\mu$m). Assessing the $f_{max}$ and $S_{half}$ on the different species groups, all species show constants that decrease with depth except for the large species where the $f_{max}$ and $S_{half}$ is high in the 50–300 m depth range (5.15–4.56 and 257.99–253.80 for $f_{max}$ and $S_{half}$, respectively) regardless of their final size (Tables 2, 4A–C). For the small species, the $f_{max}$ varies between 1.41 and 1.57, and $S_{half}$ ranges between 143.32 and 149.08 $\mu$m, while the large species show higher $f_{max}$ from 3.88 to 5.40, at a $S_{half}$ of 189.53 to 262.36 $\mu$m, respectively. For the medium-sized species, the $S_{half}$ and $f_{max}$ constants have a range between the ones observed in small to large species, with $S_{half}$ varying from 178.86 to 196.44 and $f_{max}$ from 3.02 to 3.30.

## Abundance estimation using the size-normalized catch model and Berger's "equivalent catch"

### *Abundance estimation using the size-normalized catch model*

To evaluate the performance and reliability of the size-normalized catch model correction scheme proposed in the study, the observed abundances planktonic Foraminifera data used to train the model were plotted vs. predicted total abundances of total specimens (all size categories; on the total of cytoplasm-filled and empty tests). These latter were calculated using Eq. 3 at each depth interval proposed by the size-normalized catch model in this study (Table 2) and yield slopes equal to unity for the global fit (1 : 1) (Fig. 6a). As discussed above (*see* "Sieve size and abundance" section), the only robust variable is the water depth. Both seasonality and regional variability between ocean basins were not taken into account for the following analyses. Given the limited sampling across ocean basins and seasons, the robustness of observed differences in MM parameters between these categories remains inconclusive, necessitating reliance on globally derived MM parameters across depth intervals, with depth-dependent trends emerging as the sole reliable factor. Furthermore, the training dataset is predominantly sourced from the Indian, North Atlantic, and Arctic Oceans. The number of samples for some latitudinal bands for this specific data can be low (159 samples from 60°N to 90°N; Fig. 1). Thus, comprehensive datasets necessary for generating accurate model equations are not uniformly present for each latitudinal band. The linear regression slopes are equal to one (1 ± 0.006) for samples obtained from depths between 0–50, > 50–100, and > 300–1000 m, and change to slopes of 0.96 ± 0.01 for a depth between 100 and 300 m (Fig. 6a; Supporting Information Table S3). The coefficient of determination ranges between 0.90 and 0.94 for the depth intervals between 0 and 1000 m (Fig. 6a). The skill of the model was also tested by using training dataset samples (including the outliers) and the results show that the obtained slopes are higher than the fit obtained without the outliers (Supporting Information Table S3). To validate our model calibrated without including the outliers, this size-normalized catch model was applied on the validation dataset (Retailleau 2009), with different size fractions (100–150, > 150–315, and > 315 $\mu$m) containing cytoplasm-filled and empty planktonic Foraminifera species tests. The slopes of the obtained regression lines from the observed vs. predicted abundances (i.e., our model estimates) range between 1 and 2.1 (Fig. 7a). The coefficient of determination is higher at depth intervals between 100 and 1000 m (between 0.79 and 0.83) than at shallower depth above 100 m (between 0.62 and 0.74). This correlation is attributed to the prevalence of large shell species at the surface rather than at depths as stated in Retailleau et al. 2011.

**Table 3.** Coefficients of multiplication for each size fraction and depth, and obtained using Eq. 4 on the training dataset.

| Size fraction | $f_k$ | | | |
|---|---|---|---|---|
| max ($\mu$m) | 0–50 m | > 50–100 m | > 100–300 m | > 300–1000 m |
| > 100–125 | 1 | 1 | 1 | 1 |
| > 125–150 | 1.52 | 1.45 | 1.46 | 1.44 |
| > 150–200 | 1.97 | 1.85 | 1.80 | 1.76 |
| > 200–250 | 2.19 | 2.03 | 1.95 | 1.89 |
| > 250–315 | 2.33 | 2.16 | 2.05 | 1.97 |
| > 315 | 2.44 | 2.26 | 2.11 | 2.03 |

### *Abundance estimation using Berger's "equivalent catch"*

The correction factor coined by Berger (1969)—Eq. 6—and termed "equivalent catch" was tested to the training dataset, and includes samples with known abundances for test sizes > 100 $\mu$m and split into subsamples (*see* "Model training dataset" section). The obtained regression lines from the predicted vs. the observed abundances show a positive

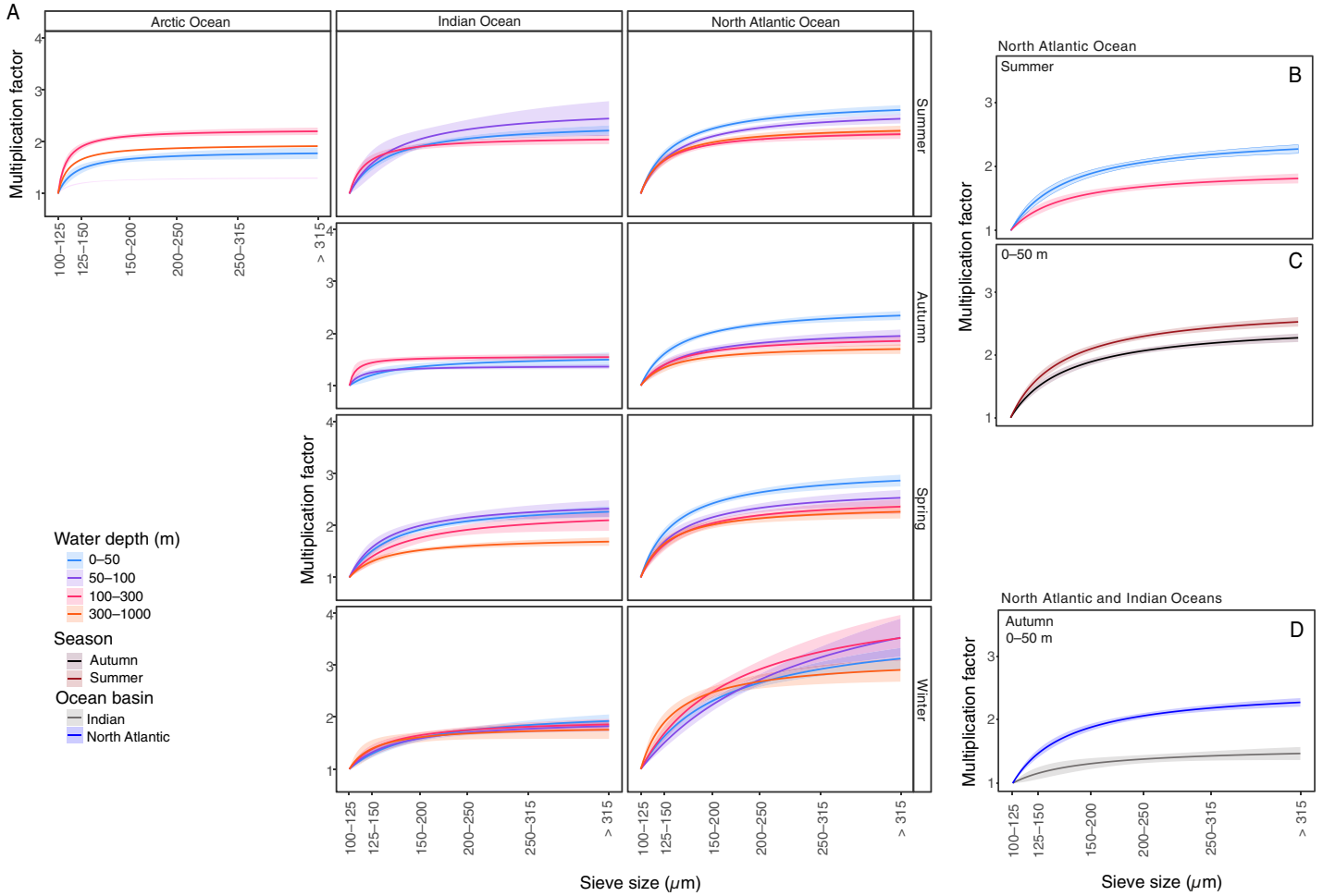


**Fig. 5.** (**a**) Multiplication factors with confidence interval derived from the cumulative abundance curves plotted vs. the different size fractions (100–125, > 125–150, > 150–200, > 200–250, > 250–315, and > 315 $\mu$m) at each depth interval, season, and ocean basin (Arctic, North Atlantic, and Indian Oceans); (**b**) in the North Atlantic Ocean at two different depths and during summer; (**c**) in the North Atlantic Ocean during autumn and summer at 0–50 m depth; and (**d**) in the North Atlantic and Indian Oceans in autumn at 0–50 m water depth. Envelopes represent confidence intervals at the limits of 2.5% and 97.5%.

relationship (Fig. 6b). Normalizing the size class > 125–200 to 100 $\mu$m results in a slope ranging between 1 and 1.3 and a coefficient of determination between 0.67 and 0.98, indicating that the predicted abundances are overestimated compared to the ones produced by the size-normalized catch model proposed in this study. However, normalizing the size class > 200–100 $\mu$m results in a slope smaller than 1 (0.22–0.92) and a low coefficient of determination that ranges between 0.26 and 0.77, that is, the predicted abundances are underestimated when using the Berger (1969) formula (Fig. 6b).

The equivalent catch approach by Berger (1969) was applied to the validation dataset from Retailleau (2009) and Retailleau et al. (2011), wherein subsample abundances were aggregated into distinct size classes (> 150 and > 315 $\mu$m). Subsequently, the cumulative sample abundances were normalized to > 100 $\mu$m using the Berger (1969) equation. Normalizing the size class > 150–315 to 100 $\mu$m yielded a slope ranging from 1.5 to 8.8 and a coefficient of determination between 0.06 and 0.94, suggesting an overestimation of predicted abundances compared to those obtained via the FORCIS size-normalized catch model (Fig. 6b).

## Discussion

### Importance of depth-dependent corrections

Our study underscores the intimate connection between MM parameters and the size and distribution of planktonic Foraminifera throughout the water column, elucidating their ecological dynamics. Our analysis reveals that foraminifera assemblages from deeper water depths have a lower multiplication factor across all size classes compared to those from shallower depths. At the same time, PF abundance decreases with depth. On the other hand, large specimens are relatively more abundant at greater depth. The MM parameters $f_{\max}$ (maximum growth potential) and $S_{\text{half}}$ (sharpness of growth)

**Table 4.** Michaelis–Menten constants $f_{max}$ and $S_{half}$ generated number of subsamples used for each water depth interval and species adult size for small (**A**), medium (**B**), and large (**C**) species.

**A. Small species**

| Depth interval (m) | $S_{half}$ ($\mu$m) | $f_{max}$ | *n* |
|---|---|---|---|
| 0–50 | 149.08 ± 4.65 | 1.57 ± 0.03 | 595 |
| > 50–100 | 150.01 ± 7.49 | 1.55 ± 0.05 | 320 |
| > 100–300 | 144.6 ± 6.11 | 1.53 ± 0.05 | 351 |
| > 300–1000 | 143.32 ± 6.54 | 1.42 ± 0.04 | 457 |

**B. Medium species**

| Depth interval (m) | $S_{half}$ ($\mu$m) | $f_{max}$ | *n* |
|---|---|---|---|
| 0–50 | 187.43 ± 5.85 | 3.30 ± 0.07 | 1444 |
| > 50–100 | 196.44 ± 9.40 | 3.27 ± 0.11 | 831 |
| > 100–300 | 178.86 ± 7.08 | 3.10 ± 0.09 | 793 |
| > 300–1000 | 180.11 ± 6.88 | 3.02 ± 0.08 | 024 |

**C. Large species**

| Depth interval (m) | $S_{half}$ ($\mu$m) | $f_{max}$ | *n* |
|---|---|---|---|
| 0–50 | 251.16 ± 17.87 | 4.87 ± 0.24 | 375 |
| > 50–100 | 257.99 ± 27.43 | 5.15 ± 0.39 | 144 |
| > 100–300 | 253.80 ± 35.74 | 4.56 ± 0.44 | 142 |
| > 300–1000 | 244.12 ± 25.13 | 4.59 ± 0.33 | 175 |

are test-size dependent. Multiplication factors vs. size class rapidly increases for small species occurring only in the two smallest size classes, and flattens out toward the larger size classes. This explains the low $S_{half}$ values assessed for the different depth ranges of the small species. Whereas the cumulative abundance of the small species is slightly decreasing with depth, the $S_{half}$ does not change across the depth ranges (Fig. 4a; Table 4a), likely because small-sized species exist at all water depths at their size limit (maximum size). For the large species, the assessed $f_{max}$ and $S_{half}$ are high and increase with depth compared to small- and medium-sized species. This implies that the larger, thus dead and heavier specimens of a species sinking, occur below the average depth of habitat of the entire population. This has been shown, for example, for *Globorotalia truncatulinoides*, which reach adult size below 100 m while their average living depth ranges above 100 m (Schiebel et al. 2002; Rebotim et al. 2017).

Overall, small specimens dominate the total planktonic Foraminifera assemblage present in the water column (Supporting Information Fig. S1), confirming previous observations (Brummer and Kroon 1988; Schiebel et al. 2002; Meilland et al. 2021). Generally, the horizontal and vertical distribution of the planktonic Foraminifera of varying size and life stages (juvenile to adult specimens) in the surface ocean changes due to mixing and passive vertical migration during the life cycle (less than 50% of all specimens that sink passively, Meilland et al. 2021). Furthermore, reproduction of different species, partly responsible for their shell sinking, may happen at different depths (Hemleben et al. 1989; Schiebel and Hemleben 2005; Meilland et al. 2021). Also, planktonic Foraminifera species' depth habitats are not the same across the different oceanic basins (Fairbanks et al. 1980; Fairbanks et al. 1982). After reproduction, empty tests rapidly sink to the seafloor (Takahashi and Bé 1984; Schiebel and Hemleben 2000). Tests of small and preadult individuals that died without reproducing slowly sink through the water column due to their low weight, being susceptible to dissolution (Bé and Hemleben 1970; Be et al. 1980; Schiebel 2002; Erez 2003; Schiebel et al. 2007; Iwasaki et al. 2019; Ofstad et al. 2021). Mass mortality of offspring shortly after reproduction may be caused by lack of food and/or predation (Brummer and Kroon 1988) and may not affect assemblages discussed here. Both juvenile mortality and reproduction at random depth for a part of the population explains the presence of small specimens (100–150 $\mu$m) in the entire surface mixed layer of the ocean (Meilland et al. 2021, 2022).

The medium size classes (200–300 $\mu$m) encompass various ontogenetic stages, including both mature adults and specimens that have not yet reached full maturity. The abundance within these classes exhibits slight variations with depth. Furthermore, it seems that the decline of abundance with depth is related to dissolution (Schiebel et al. 2007), habitat preference (Mortyn and Charles 2003; Jonkers and Kučera 2015), or specimens that reduce in number from the system, and, for example, end up in predator guts (Bradbury and Castro 1971; Brand and Lipps 1982). In waters deeper than 300 m, almost all planktonic Foraminifera tests are empty (Berger 1969; Schiebel 2002). Our findings highlight the critical importance of using depth-normalized MM parameters to accurately capture variations in planktonic Foraminifera populations. The observed size and depth-dependent differences in PF distribution underscore the necessity of accounting for these ecological dynamics when estimating normalized abundances.

### The FORCIS correction—Application, limitation, and benefits for the entire plankton community

The FORCIS size-normalized catch model was applied to normalize the total abundance of the CPR and plankton tow abundances data of the FORCIS database to a 100 $\mu$m mesh size (Fig. 8). The constants $f_{max}$ and $S_{half}$ for the FORCIS abundance-size corrections were used according to the sample depth and for the total number of specimens (cytoplasm-filled and empty specimens) from all size classes (Table 2). When this size-normalized catch model is applied to the FORCIS database at all depths, using the MM parameters generated for each depth interval, and binned at each 4.3° latitude by 8.6° longitude, the resulting map (Fig. 8) shows that the standardized abundances normalized to 100 $\mu$m mesh size is between 1 and $10^3$ ind m$^{-3}$. In addition, applying the size-normalized

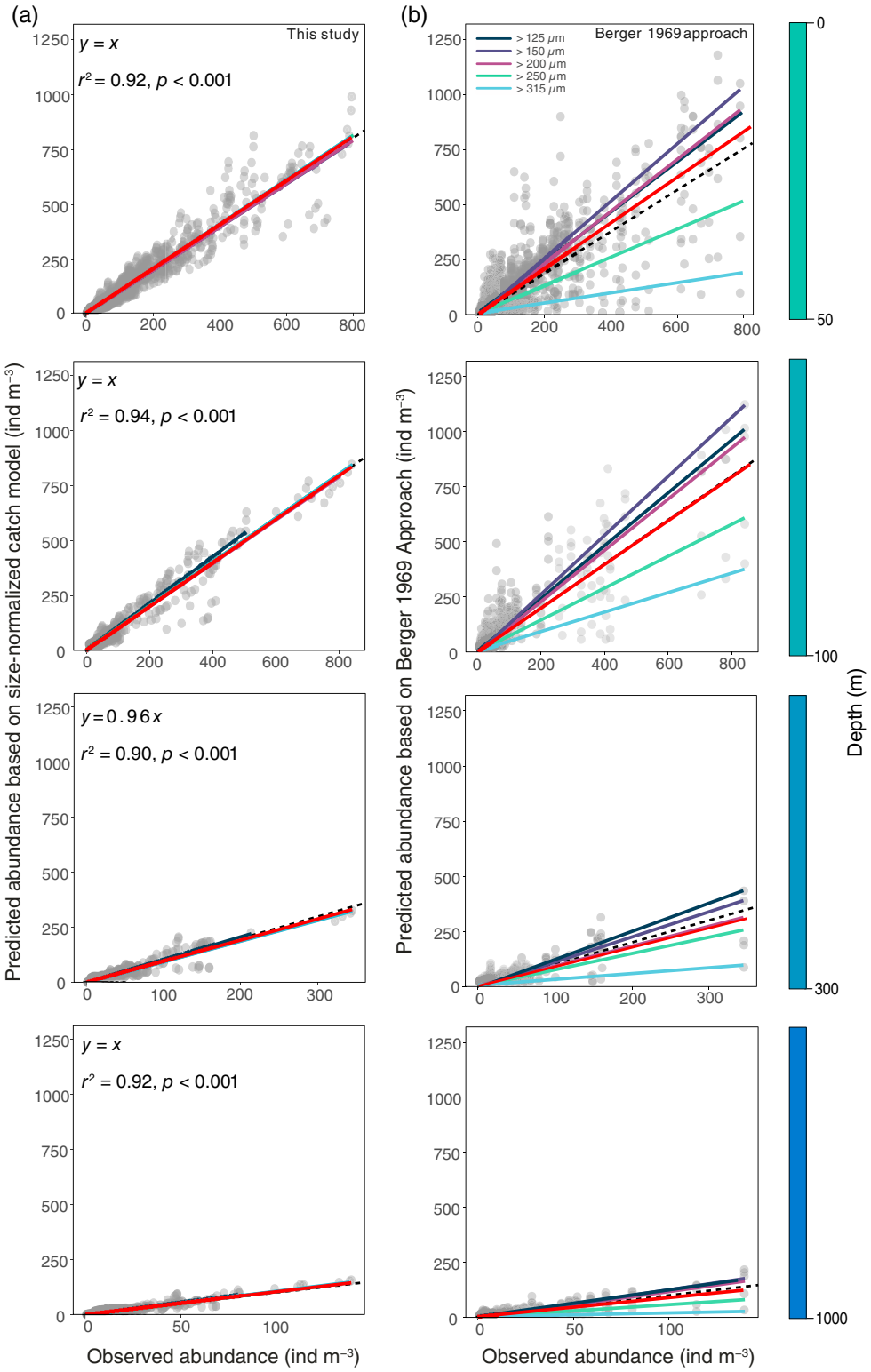


**Fig. 6.** Comparison of observed abundances from the training datasets at various size fractions (> 125–150, > 150–200, > 200–250, > 250–315, and > 315 $\mu$m) against estimated abundances obtained using size-normalized catch model proposed for different water depth intervals (0–50, 50–100, 100–300, and 300–1000 m) (**a**) and, linear regressions between observed abundance the training dataset data in the size fraction above 100 $\mu$m and abundances obtained with mesh sizes above 125 $\mu$m (dark blue line), 150 $\mu$m (purple line), 200 $\mu$m (pink line), 250 $\mu$m (green line), and 315 $\mu$m (light blue line) across different depth ranges (0–50, > 50–100, > 100–300, and > 300–1000 m), standardized to 100 $\mu$m using Eq. 6 (Berger 1969) (**b**). Red lines represent the linear regressions of all fractions from the training datasets at the different water depth intervals.

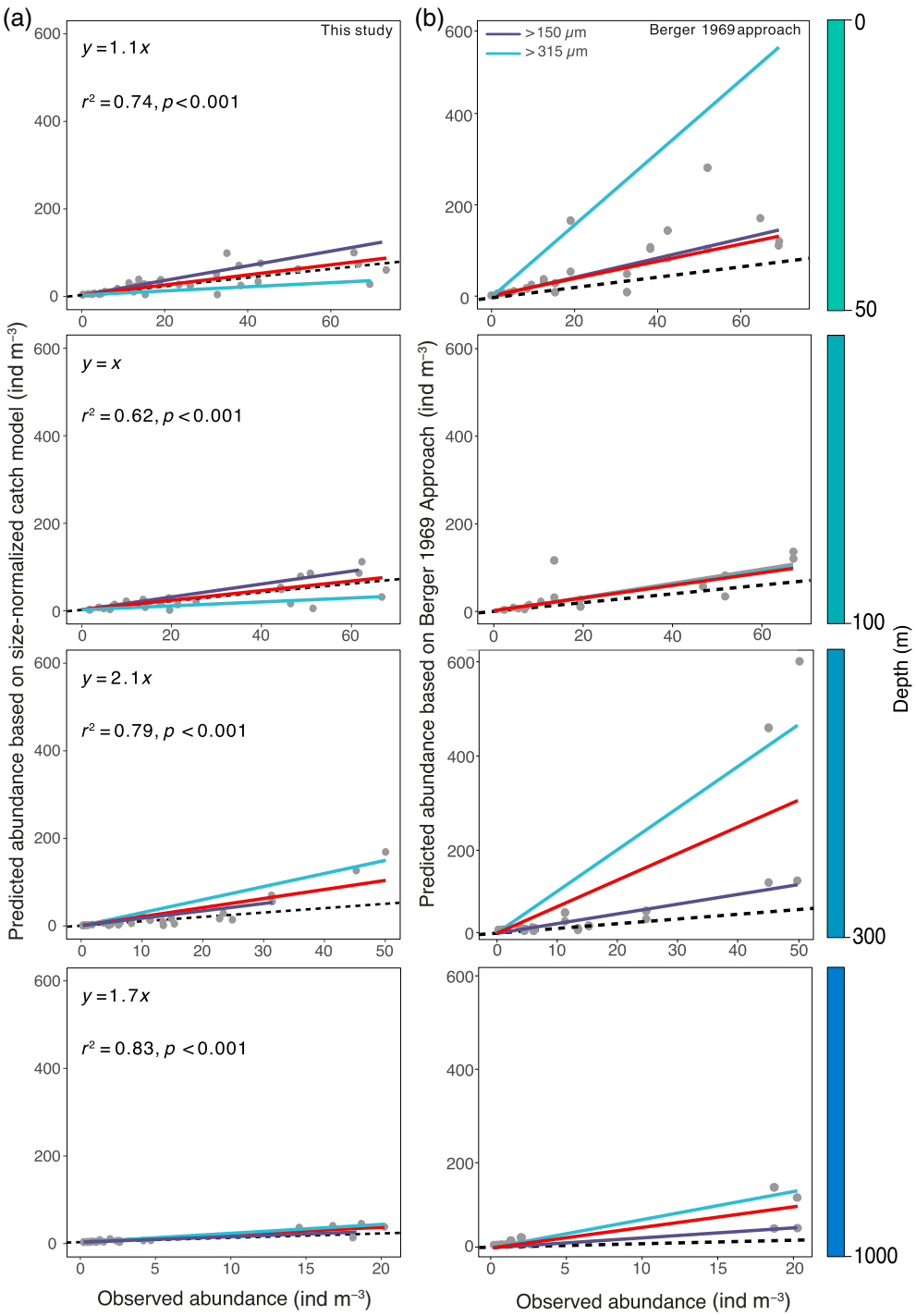


**Fig. 7.** Observed abundances from an independent dataset (Retailleau et al. 2011) at each size fraction (> 150–315 and > 315 $\mu$m) vs. the estimated ones obtained using the size-normalized catch model proposed for each depth interval (0–50, 50–100, > 100–300, and > 300–1000 m) (**a**) and, linear regressions between observed abundance from an independent dataset (Retailleau et al. 2011) in the size fraction above 100 $\mu$m and abundances obtained with mesh sizes above 150 $\mu$m (purple line) and 315 $\mu$m (light blue line) across different depth ranges (0–50, > 50–100, > 100–300, and > 300–1000 m), standardized to 100 $\mu$m using Eq. 6 (Berger 1969) (**b**). Red lines represent the linear regressions of all fractions from the independent dataset (Retailleau et al. 2011) at the different water depth intervals.

catch model proposed in this study on independent dataset that have not been used to generate the applied model, the predicted abundances are close to the observed ones (Fig. 7a). The linear regression between the observed and predicted abundances presents slopes very close to 1 (1–1.4), and coefficients of determination higher than 0.46. This precision is

somewhat reduced at the surface due to larger specimens, particularly near continental shelves, which may reflect inhibited reproduction in neritic conditions (Retailleau et al. 2011).

When applying the Berger (1969) correction (Eq. 6), the estimated abundances are generally overestimated compared to the FORCIS abundance-size correction (Figs. 6b, 7b). The FORCIS abundance-size correction method, developed in this study for planktonic Foraminifera offers a reliable ubiquitous approach to estimate the abundance of foraminifera > 100 $\mu$m across water depth ranges to normalize abundances of planktonic Foraminifera retrieved using different sieve or mesh sizes. The applicability of this correction method can be successfully transferred to a wide range of other planktonic groups, including radiolaria, diatoms, acantharia, and dinoflagellates, that follow similar cumulative abundance vs. size distribution as the planktonic Foraminifera in the water column, whose sampling techniques are also based on a variety of plankton nets mesh sizes. However, the FORCIS correction method would need a calibration step on a size-fractionated subset for each new plankton group, and may provide accurate and standardized estimates of abundances. This may enable better comparison and analyses across studies and contribute to an improved understanding of the ecological significance in marine ecosystems.

However, the technique has some limitations. For instance, if the abundance is null in one of the size fractions > 100 $\mu$m (i.e., $C_k = 0$), it is not possible to derive the abundance using Supporting Information Eq. S2 in the adjacent size-fraction bin and impede estimation of the total abundance ($C_{tot}$). When deriving the FORCIS size-normalized catch model for a specific taxon, it is essential to carefully select the suitable model. Particularly, the inclusion of taxa with diverse size spectra and adequate occurrence becomes imperative. Complications may arise when dealing with rare species or taxa that exhibit narrow size ranges. For instance, the species *Orcadia riedeli* is a rare planktonic Foraminifera species (Holmes 1984; Brummer and Kroon 1988; Meilland et al. 2018) with a narrow size spectrum between 100 and 150 $\mu$m in the FORCIS dataset. When applying the size-normalized catch model to *O. riedeli* to reconstruct the coefficients of multiplication $f_k$ for each size fraction (100–125 and >125–150 $\mu$m) and water depth interval, the obtained curve is flat with a very low multiplication factor. The challenge lies in accurately predicting the abundance of small species when working with data primarily

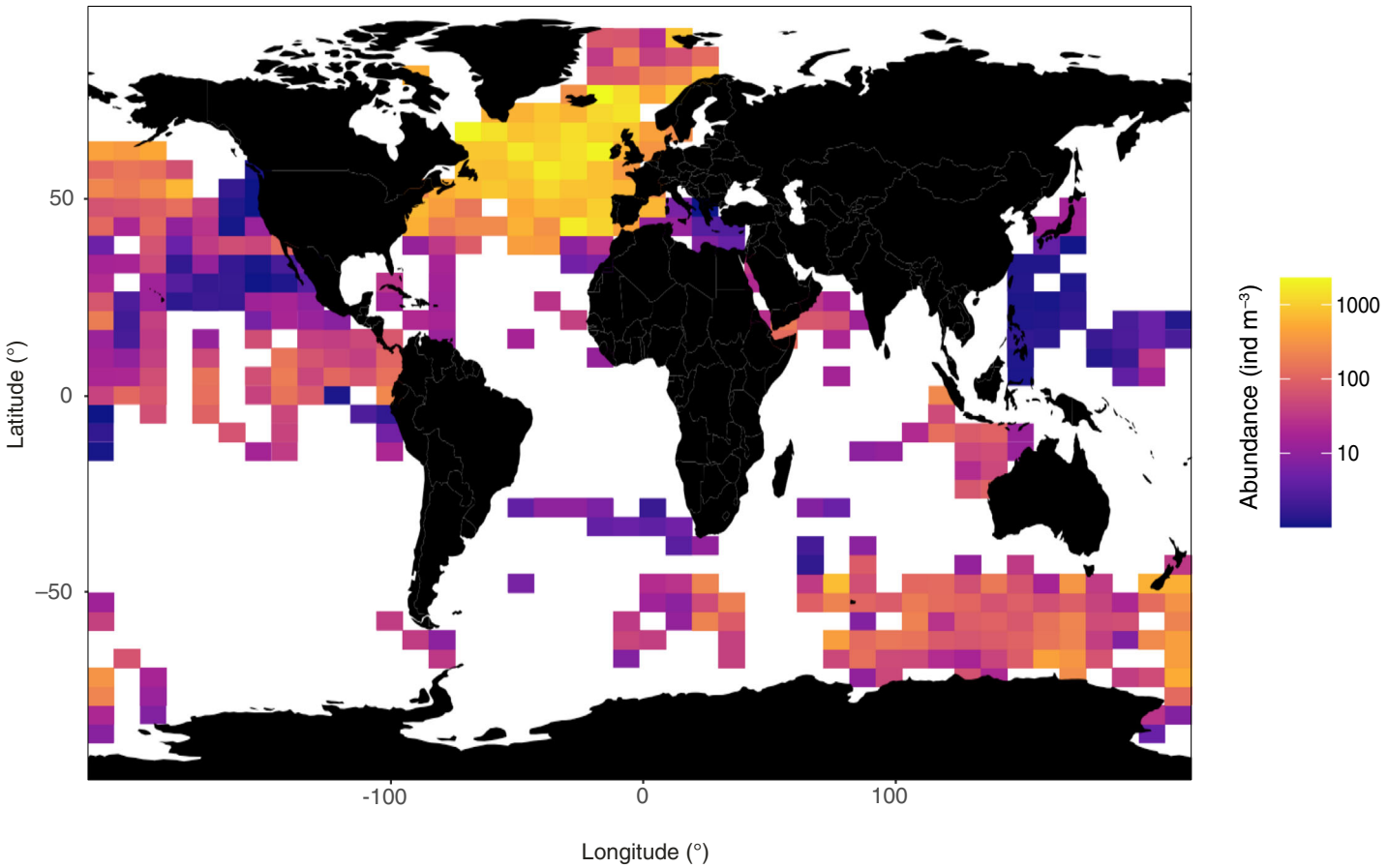


**Fig. 8.** Global (FORCIS data) planktonic Foraminifera abundance averaged over 4.3° latitude by 8.6° longitude bands over the entire water column (0–1000 m) obtained from plankton nets and CPRs, standardized to 100 $\mu$m using the size-normalized catch model proposed in this study.

focused on large sizes. Applying a generic equation for small species may not suffice due to potential limitations in observing them within the larger size classes. Therefore, the model proposed here produces best results for size-abundance on taxa with a wide size spectrum, ranging from juveniles to adult individuals. By including data across different life stages, a more comprehensive understanding of the size–number relationship may be achieved.

### *Final comments and recommendations*

Planktonic Foraminifera test size varies according to different parameters such as species, ontogenetic stage, and ecological factors including trophic conditions and water depth habitat. The FORCIS database, used in this study, assembles abundances of specimens collected with different devices and mesh sizes over the past 125 yr, which affects the estimation of their abundance. To mitigate discrepancies arising from these varied sampling methods, a correction factor was derived from abundance data of size-fractionated planktonic Foraminifera samples that underwent sieve-splitting post-collection. The resulting relationships present a general asymptotic shape, which we model using Michaelis–Menten-like fits across different water depth intervals (0–50, > 50–100, > 100–300, > 300–1000, and > 1000 m). Using these relationships, the abundance of planktonic Foraminifera larger than 100 $\mu$m can be assessed to normalize the global abundance dataset of the FORCIS database.

The methodology proposed here proves to be more accurate than the initial correction scheme proposed by Berger (1969), leveraging a much larger calibration dataset. Unlike Berger's method, which tends to overestimate abundance in the 125–200 $\mu$m size fraction, and underestimate in the larger than 200 $\mu$m size fractions, our comprehensive training dataset enables the development of a size-normalized catch model applicable not only to Foraminifera but potentially to other planktonic groups.

Emphasizing the adoption of a standard 100 $\mu$m size criterion for future planktonic Foraminifera research could eliminate the need for such corrections, promoting consistency and comparability across studies. This standardization is critical for advancing our understanding of planktonic Foraminifera populations within marine ecosystems.

### Data availability statement

All data associated with this article and codes to generate the FORCIS size-normalized catch model are available Zenodo through this link: https://doi.org/10.5281/zenodo.7437719.

## References


Anderson, D. M., and W. L. Prell. 1993. A 300 kyr record of upwelling off Oman during the Late Quaternary: Evidence of the Asian southwest monsoon. Paleoceanography **8**: 193–208. doi:10.1029/93PA00256

Bé, A. 1977. An ecological, zoogeographic and taxonomic review of recent planktonic Foraminifera, p. 1–100. Oceanic Micropalaeontol. Academic Press. doi:10.1126/science.198.4320.924

Bé, A. W. H., and O. R. Anderson. 1976. Gametogenesis in planktonic Foraminifera. Science **192**: 890–892. doi:10.1126/science.946914

Bé, A. W. H., and C. Hemleben. 1970. Calcification in a living planktonic foraminifer, *Globigerinoides sacculifer* (Brady). Neues Jahrb. Geol. Palaeontol. **134**: 221–234.

Bé, A. W. H., and W. H. Hutson. 1977. Ecology of planktonic Foraminifera and biogeographic patterns of life and fossil assemblages in the Indian Ocean. Micropaleontology **23**: 369. doi:10.2307/1485406

Be, A. W. H., C. Hemleben, O. R. Anderson, and M. Spindler. 1980. Pore structures in planktonic Foraminifera. J. Foraminiferal Res. **10**: 117–128. doi:10.2113/gsjfr.10.2.117

Bé, A. W. H., J. K. B. Bishop, M. S. Sverdlove, and W. D. Gardner. 1985. Standing stock, vertical distribution and flux of planktonic Foraminifera in the Panama basin. Mar. Micropaleontol. **9**: 307–333. doi:10.1016/0377-8398(85)90002-7

Berger, W. H. 1969. Ecologic patterns of living planktonic Foraminifera. Deep. Res. Oceanogr. Abstr. **16**: 1–24. doi:10.1016/0011-7471(69)90047-3

Berger, W. H. 1971. Sedimentation of planktonic Foraminifera. Mar. Geol. **11**: 325–358. doi:10.1016/0025-3227(71)90035-1

Bernhard, J. M. 2000. Distinguishing live from dead Foraminifera: Methods review and proper applications. Micropaleontology **46**: 38–46. doi:10.2307/1486179

Boltovskoy, E., D. Boltovskoy, and F. Brandini. 2000. Planktonic Foraminifera from south-western Atlantic epipelagic waters: Abundance, distribution and year-to-year variations. J. Mar. Biol. Assoc. UK **80**: 203–213. doi:10.1017/S0025315499001794

Bonneau, M. C., F. Melieres, and C. Vergnaud-Grazzini. 1980. Variations isotopiques (oxygène et carbone) et cristallographiques chez des espèces actuelles de foraminifères planctoniques en fonction de la profondeur de dépôt. Bull. Soc. Géol. Fr. **22**: 791–793. doi:10.2113/gssgfbull.S7-XXII.5.791

Bradbury, L. J. S., and I. P. Castro. 1971. A pulsed-wire technique for velocity measurements in highly turbulent flows. J. Fluid Mech. **49**: 657–691. doi:10.1017/S0022112071002313

Brand, T. E., and J. H. Lipps. 1982. Foraminifera in the trophic structure of shallow-water Antarctic marine communities. J. Foraminiferal Res. **12**: 96–104. doi:10.2113/gsjfr.12.2.96

Brummer, G.-J. A., C. Hemleben, and M. Spindler. 1987. Ontogeny of extant spinose planktonic Foraminifera (Globigerinidae): A concept exemplified by *Globigerinoides sacculifer* (Brady) and *G. Ruber* (d'Orbigny). Mar.

Micropaleontol. **12**: 357–381. doi:10.1016/0377-8398(87)90028-4

Brummer, J. A., and D. Kroon. 1988. Comparative ontogeny and species definition of planktonic foraminifers: A case study of *Dentigloborotalia anfracta* n.gen, p. 51–57. *In* Planktonic Foraminifers as tracers of ocean-climate history. Free Univ. Press.

Brummer, G.-J. A., and M. Kučera. 2022. Taxonomic review of living planktonic Foraminifera. J. Micropalaeontol. **41**: 29–74. doi:10.5194/jm-41-29-2022

Caulet, J. P., M. T. Vénec-Peyré, C. Vergnaud-Grazzini, and C. Nigrini. 1992. Variation of South Somalian upwelling during the last 160 ka: Radiolarian and Foraminifera records in core MD 85674. Geol. Soc. Spec. Publ. **64**: 379–389. doi:10.1144/GSL.SP.1992.064.01.25

Chaabane, S., and others. 2023. The FORCIS database: A global census of planktonic Foraminifera from ocean waters. Sci. Data **10**: 354. doi:10.1038/s41597-023-02264-2

CLIMAP. 1976. The surface of the ice-age earth. Science **191**: 1131–1137. doi:10.1126/science.191.4232.1131

Corliss, B. H., and S. Emerson. 1990. Distribution of rose bengal stained deep-sea benthic Foraminifera from the Nova Scotian continental margin and gulf of Maine. Deep Sea Res. A Oceanogr. Res. Pap. **37**: 381–400. doi:10.1016/0198-0149(90)90015-N

de Garidel-Thoron, T., Y. Rosenthal, F. Bassinot, and L. Beaufort. 2005. Stable sea surface temperatures in the western Pacific warm pool over the past 1.75 million years. Nature **433**: 1–5. doi:10.1038/nature03189

de Garidel-Thoron, T., and others. 2022. The foraminiferal response to climate stressors project: Tracking the community response of planktonic Foraminifera to historical climate change. Front. Mar. Sci. **9**: 1–6. doi:10.3389/fmars.2022.827962

Erez, J. 2003. The source of ions for biomineralization in Foraminifera and their implications for paleoceanographic proxies. Rev. Mineral. Geochem. **54**: 115–149. doi:10.2113/0540115

Fairbanks, R. G., P. H. Wiebe, and A. W. H. Bé. 1980. Vertical distribution and isotopic composition of living planktonic Foraminifera in the western north Atlantic. Science **207**: 61–63. doi:10.1126/science.207.4426.61

Fairbanks, R. G., M. Sverdlove, R. Free, P. H. Wiebe, and A. W. H. Bé. 1982. Vertical distribution and isotopic fractionation of living planktonic Foraminifera from the Panama Basin. Nature **298**: 841–844. doi:10.1038/298841a0

Freedman, D., R. Pisani, and R. Purves. 2007. Statistics. W. W. Norton & Company.

Ganssen, G. 1991. Years (1984, 1985) throughout the Red Sea, reveal two. Earth **6**: 73–82. doi:10.1029/90PA01976

Grazzini, C. V., M. T. Vénec-peyré, J. P. Caulet, and N. Lerasle. 1995. Fertility tracers and monsoon forcing at an equatorial site of the Somali Basin (Northwest Indian Ocean). Mar. Micropaleontol. **26**: 137–152. doi:10.1016/0377-8398(95)00070-4

Hecht, A. 1976. An ecologic model for test size variation in recent planktonic Foraminifera; applications to the fossil record. J. Foraminifer. Res. **6**: 295–311. doi:10.2113/gsjfr.6.4.295

Hemleben, C., M. Spindler, and O. Anderson. 1989. Modern planktonic Foraminifera, 363 pp. Springer-Verlag.

Hohenegger, J., A. Briguglio, and W. Eder. 2014. The natural laboratory of algal symbiont-bearing benthic Foraminifera: Studying individual growth and population dynamics in the sublittoral, p. 13–28. *In* H. Kitazato and J. M. Bernhard [eds.], Approaches to study living Foraminifera: Collection, maintenance and experimentation. Springer. doi:10.1007/978-4-431-54388-6_2

Holmes, N. A. 1984. An emendation of the genera *Beella* Banner and Blow, 1960, and *Turborotalita* Blow and Banner, 1962; with notes on *Orcadia* Boltovskoy and Watanabe, 1982. J. Foraminifer. Res. **14**: 101–110. doi:10.2113/gsjfr.14.2.101

Iwasaki, S., K. Kimoto, O. Sasaki, H. Kano, and H. Uchida. 2019. Sensitivity of planktic foraminiferal test bulk density to ocean acidification. Sci. Rep. **9**: 1–9. doi:10.1038/s41598-019-46041-x

Johnson, K. A., and R. S. Goody. 2011. The original Michaelis constant: Translation of the 1913 Michaelis–Menten paper. Biochemistry **50**: 8264–8269. doi:10.1021/bi201284u

Jonkers, L., and M. Kučera. 2015. Global analysis of seasonality in the shell flux of extant planktonic Foraminifera. Biogeosciences **12**: 2207–2226. doi:10.5194/bg-12-2207-2015

Keigwin, L., M. Bice, and N. Copley. 2005. Seasonality and stable isotopes in planktonic Foraminifera off Cape Cod, Massachusetts. Paleoceanography **20**. doi:10.1029/2005PA001150

King, J. E., and J. Demond. 1953. Zooplankton abundance in the Central Pacific. Fish. Bull. **82**: 11–144.

Kroon, D., and G. Ganssen. 1989. Northern Indian Ocean upwelling cells and the stable isotope composition of living planktonic foraminifers. Deep Sea Res. A Oceanogr. Res. Pap. **36**: 1219–1236. doi:10.1016/0198-0149(89)90102-7

Kucera, M., A. Rosell-Melé, R. Schneider, C. Waelbroeck, and M. Weinelt. 2005. Multiproxy approach for the reconstruction of the glacial ocean surface (MARGO). Quat. Sci. Rev. **24**: 813–819. doi:10.1016/j.quascirev.2004.07.017

Kuroyanagi, A., and H. Kawahata. 2004. Vertical distribution of living planktonic Foraminifera in the seas around Japan. Mar. Micropaleontol. **53**: 173–196. doi:10.1016/j.marmicro.2004.06.001

Lessa, D., R. Morard, L. Jonkers, I. M. Venancio, R. Reuter, A. Baumeister, A. L. Albuquerque, and M. Kučera. 2020. Distribution of planktonic Foraminifera in the subtropical South Atlantic: Depth hierarchy of controlling factors. Biogeosciences **17**: 4313–4342. doi:10.5194/bg-17-4313-2020

Mallo, M., P. Ziveri, P. Graham Mortyn, R. Schiebel, and M. Grelaud. 2017. Low planktic foraminiferal diversity and

abundance observed in a spring 2013 west-east Mediterranean Sea plankton tow transect. Biogeosciences **14**: 2245–2266. doi:10.5194/bg-14-2245-2017

Meilland, J., R. Schiebel, C. Lo Monaco, S. Sanchez, and H. Howa. 2018. Abundances and test weights of living planktic foraminifers across the Southwest Indian Ocean: Implications for carbon fluxes. Deep Res. I Oceanogr. Res. Pap. **131**: 27–40. doi:10.1016/j.dsr.2017.11.004

Meilland, J., M. Siccha, M. Kaffenberger, J. Bijma, and M. Kucera. 2021. Population dynamics and reproduction strategies of planktonic Foraminifera in the open ocean. Biogeosciences **18**: 5789–5809. doi:10.5194/bg-18-5789-2021

Meilland, J., M. M. Ezat, A. Westgard, C. Manno, R. Morard, M. Siccha, and M. Kucera. 2022. Rare but persistent asexual reproduction explains the success of planktonic Foraminifera in polar oceans. J. Plankton Res. **45**: fbac069. doi:10.1093/plankt/fbac069

Michaelis, L., and M. L. Menten. 1913. Die kinetik der invertinwirkung. Biochemistry **49**: 352.

Mortyn, P. G., and C. D. Charles. 2003. Planktonic foraminiferal depth habitat and $\delta^{18}O$ calibrations: Plankton tow results from the Atlantic sector of the Southern Ocean. Paleoceanography **18**: 1–15. doi:10.1029/2001PA000637

Mortyn, P. G., and M. A. Martinez-Boti. 2007. Planktonic Foraminifera and their proxies for the reconstruction of the surface-ocean climate parameters. Contrib. Sci. **3**: 371–383. doi:10.2436/20.7010.01.14

Ofstad, S., K. Zamelczyk, K. Kimoto, M. Chierici, A. Fransson, and T. L. Rasmussen. 2021. Shell density of planktonic Foraminifera and pteropod species *Limacina helicina* in the Barents Sea: Relation to ontogeny and water chemistry. PLoS One **16**: 1–24. doi:10.1371/journal.pone.0249178

Peeters, F., E. Ivanova, S. Conan, G. J. Brummer, G. Ganssen, S. Troelstra, and J. Van Hinte. 1999. A size analysis of planktic Foraminifera from the Arabian Sea. Mar. Micropaleontol. **36**: 31–63. doi:10.1016/S0377-8398(98)00026-7

R Core Team. 2021. R: A language and environment for statistical computing. R Foundation for Statistical Computing. doi:5400 10.32614/CRAN.package.exams

Rebotim, A., A. H. L. Voelker, L. Jonkers, J. J. Waniek, H. Meggers, R. Schiebel, I. Fraile, M. Schulz, and M. Kucera. 2017. Factors controlling the depth habitat of planktonic Foraminifera in the subtropical eastern North Atlantic. Biogeosciences **14**: 827–859. doi:10.5194/bg-14-827-2017

Retailleau, S. 2009. Ecologie des foraminifères planctoniques du golfe de Gascogne: Variations spatiotemporelles des assemblages et géochimie de leurs tests. Doctoral dissertation. Planète et Univers [Physics], Univ. d'Angers. Available from http://tel.archives-ouvertes.fr/tel-00480660

Retailleau, S., R. Schiebel, and H. Howa. 2011. Population dynamics of living planktic foraminifers in the hemipelagic southeastern Bay of Biscay. Mar. Micropaleontol. **80**: 89–100. doi:10.1016/j.marmicro.2011.06.003

Ritz, C., F. Baty, J. C. Streibig, and D. Gerhard. 2015. Dose-response analysis using R. PLoS One **10**: e0146021. doi:10.1371/journal.pone.0146021

Sardari, D. 2023. Chapter 5: Mathematical basis for diatom growth modeling. *In* J. L. Pappas [ed.], The mathematical biology of diatoms. Scrivener Publishing LLC. doi:10.1002/9781119751939.ch5

Schiebel, R. 2002. Planktic foraminiferal sedimentation and the marine calcite budget. Global Biogeochem. Cycles **16**: 3-1–3-21. doi:10.1029/2001gb001459

Schiebel, R., B. Hiller, and C. Hemleben. 1995. Impacts of storms on recent planktic foraminiferal test production and $CaCO_3$ flux in the North Atlantic at 47°N, 20°W (JGOFS). Mar. Micropaleontol. **26**: 115–129. doi:10.1016/0377-8398(95)00035-6

Schiebel, R., and C. Hemleben. 2000. Interannual variability of planktic foraminiferal populations and test flux in the eastern North Atlantic Ocean (JGOFS). Deep Res. II Top. Stud. Oceanogr. **47**: 1809–1852. doi:10.1016/S0967-0645(00)00008-4

Schiebel, R., J. Waniek, A. Zeltner, and M. Alves. 2002. Impact of the Azores front on the distribution of planktic foraminifers, shelled gastropods, and coccolithophorids. Deep Res. II Top. Stud. Oceanogr. **49**: 4035–4050. doi:10.1016/S0967-0645(02)00141-8

Schiebel, R., and C. Hemleben. 2005. Modern planktic Foraminifera. Paläontol. Z. **79**: 135–148. doi:10.1007/BF03021758

Schiebel, R., S. Barker, R. Lendt, H. Thomas, and J. Bollmann. 2007. Planktic foraminiferal dissolution in the twilight zone. Deep Sea Res. II Top. Stud. Oceanogr. **54**: 676–686. doi:10.1016/j.dsr2.2007.01.009

Schiebel, R., and C. Hemleben. 2017. Planktic foraminifers in the modern ocean. p. 1–358. Springer. doi:10.1007/978-3-662-50297-6

Schmidt, D. N., S. Renaud, J. Bollmann, R. Schiebel, and H. R. Thierstein. 2004. Size distribution of Holocene planktic foraminifer assemblages: Biogeography, ecology and adaptation. Mar. Micropaleontol. **50**: 319–338. doi:10.1016/S0377-8398(03)00098-7

Sousa, S. H. M., S. S. de Godoi, P. G. C. Amaral, T. M. Vicente, M. V. A. Martins, M. R. G. S. Sorano, S. A. Gaeta, R. F. Passos, and M. M. Mahiques. 2014. Distribution of living planktonic Foraminifera in relation to oceanic processes on the southeastern continental Brazilian margin (23°S–25°S and 40°W–44°W). Cont. Shelf Res. **89**: 76–87. doi:10.1016/j.csr.2013.11.027

Steens, T. N. F., G. Ganssen, and D. Kroon. 1992. Oxygen and carbon isotopes in planktonic Foraminifera as indicators of upwelling intensity and upwelling-induced high productivity in sediments from the northwestern Arabian Sea. Geol. Soc. Spec. Publ. **64**: 107–119. doi:10.1144/GSL.SP.1992.064.01.07

Strack, A., L. Jonkers, M. C. Rillo, H. Hillebrand, and M. Kucera. 2022. Plankton response to global warming is characterized by non-uniform shifts in assemblage composition

since the last ice age. Nat. Ecol. Evol. **6**: 1–10. doi:10.1038/s41559-022-01888-8

Sverdlove, M. S., and A. W. H. Bé. 1985. Taxonomic and ecological significance of embryonic and juvenile planktonic Foraminifera. J. Foraminiferal Res. **15**: 235–241. doi:10.2113/gsjfr.15.4.235

Takahashi, K., and A. W. H. Bé. 1984. Planktonic Foraminifera: Factors controlling sinking speeds. Deep Sea Res. A Oceanogr. Res. Pap. **31**: 1477–1500. doi:10.1016/0198-0149(84)90083-9

Ufkes, E., J. H. F. Jansen, and G. J. A. Brummer. 1998. Living planktonic Foraminifera in the eastern South Atlantic during spring: Indicators of water masses, upwelling and the Congo (Zaire) river plume. Mar. Micropaleontol. **33**: 27–53. doi:10.1016/S0377-8398(97)00032-7

Walters, W. A., C. Ley, T. Hastie, R. E. Ley, and J. Parsonnet. 2024. A modified Michaelis–Menten equation estimates growth from birth to 3 years in healthy babies in the USA. BMC Med. Res. Methodol. **24**: 27. doi:10.1186/s12874-024-02145-1

## Acknowledgments

The FORCIS project is supported by the French Foundation for Biodiversity Research (FRB) (https://www.fondationbiodiversite.fr/) within the Centre for the Synthesis and Analysis of Biodiversity (CESAB) (https://www.fondationbiodiversite.fr/la-fondation/le-cesab/) and co-funded by INSU-CNRS LEFE program, and the Max Planck Institute for Chemistry (MPIC) in Mainz. This work received support from the French government under the France 2030 investment plan, as part of the Initiative d'Excellence d'Aix-Marseille Université—A*MIDEX (AMX-19-IET-012) to ITEM project RapMed.

## Conflict of Interest

None declared.

*Submitted 13 March 2024*
*Revised 15 June 2024*
*Accepted 19 June 2024*

*Associate editor: Gordon T. Taylor*